A Study of Heat-Treatment Induced Framework Contraction in Strontium-ETS-4 by Powder Neutron Diffraction and Vibrational Spectroscopy

Sankar Nair,[†] Michael Tsapatsis,*[,†] Brian H. Toby,[‡] and Steven M. Kuznicki[§]

Contribution from the Department of Chemical Engineering, University of Massachusetts Amherst, Amherst Massachusetts 01003-9303, Center for Neutron Research, National Institute of Standards and Technology, Gaithersburg Maryland 20899, and Engelhard Corporation, Iselin New Jersey 08830-0770

Received July 12, 2001

Abstract: The effects of heat-treatment on the structure of the strontium ion-exchanged titanosilicate ETS-4 have been studied by Rietveld analysis of powder neutron diffraction data and by FT-Raman spectroscopy. Hydrous Sr-ETS-4 (space group *Cmmm*), upon heat-treatment under inert atmosphere at temperatures between 423 and 573 K, exhibits framework contraction as evinced by the decrease in the unit cell dimensions. The effects of heat-treatment on the dimensions of the transport-controlling eight-membered ring (8MR) are elucidated by Rietveld analysis. It is also found that during heat-treatment: (a) the double three membered rings (D3MRs) in ETS-4 are sites of structural instability, (b) the titania chains running along [010] exhibit a large degree of disorder in the bridging oxygen atoms, and (c) significant relocations of the strontium cations take place, which may affect the separation properties of the heat-treated materials. Raman spectra of heat-treated ETS-4 crystals exhibit strong cation−framework interaction effects. Vibrational modes involving the atoms in the titania chains show progressive frequency shifts and loss of intensity with increasing heat-treatment temperature, in a manner consistent with the crystallographic results. The study indicates the potential for continuously varying the effective pore dimension of ETS-4 by combining heat-treatment with appropriate ion-exchange procedures.

Introduction

Engelhard titanosilicate-4 (ETS-4) is a mixed oxide microporous molecular sieve material containing octahedral (six-coordinated) and square-pyramidal (five-coordinated) titanate structural units, in addition to the tetrahedral silicate units found in conventional zeolitic materials. A related titanosilicate material, ETS-10,[1,2] has potential applications in catalysis.[3,4] ETS-10 is also a wide-gap semiconductor, as indicated by UV diffuse reflectance measurements and electronic band structure calculations.[5−7] Semiconductivity in ETS-10 and related structures such as ETS-4, is attributed to the presence of titania chains in which the titanium atom is octahedrally coordinated. In ETS-10, these chains propagate along the [100] and [010] directions, and are separated from each other by tetrahedral silicate units. They are capable of 1-D quantum electron confinement with an effective electron mass (μ) of 1.66−1.97 m_e, and therefore constitute atomically defined 1-D quantum nanowires embedded in an insulating silicate matrix.

The material ETS-4 shares some structural features with ETS-10 but has received less attention in the literature. This is possibly because of the low thermal stability of the as-synthesized form (Na-ETS-4),[8,9] which occludes sodium cations (besides water molecules) in the void space. The ETS-4 framework (Figure 1a,b) can be considered as being built from titania chains propagating in the [010] direction, and bridged by titanosilicate units connecting the chains in the [100] direction. The chains contain octahedrally coordinated titanium, and are connected by means of silicate tetrahedra in the [001] direction. The bridging unit consists of a five-coordinated titanium atom, which is bonded to four silicate tetrahedra and to an apical oxygen atom, in a square-planar configuration.[10] Although a six-coordinated environment has also been assumed[11] for the titanium in the bridging unit, its five-coordinated environment has recently been confirmed by a structure solution from single-crystal X-ray data.[12] The bridging units are connected to the titania

* Corresponding author. E-mail: tsapatsi@ecs.umass.edu.
† University of Massachusetts Amherst.
‡ Center for Neutron Research, National Institute of Standards and Technology.
§ Engelhard Corporation.

(1) Kuznicki, S. M. U.S. Patent 4,853,202, 1989.
(2) Anderson, M. W.; Terasaki, O.; Ohsuna, T.; O'Malley, P. J.; Philippou, A.; Mackay, S. P.; Ferreira, A.; Rocha, J.; Lidin, S. *Philos. Mag. B* **1995**, *71*, 813.
(3) Das, T. K.; Chandwadkar, A. J.; Sivasanker, S. *J. Mol. Catal. A* **1996**, *107*, 199.
(4) Philippou, A.; Naderi, M.; Rocha, J.; Anderson, M. W. *Catal. Lett.* **1998**, *53*, 221.
(5) Borello, E.; Lamberti, C.; Bordiga, S.; Zecchina, A. *Appl. Phys. Lett.* **1997**, *71* (16), 2319.
(6) Lamberti, C. *Microporous Mesoporous Mater.* **1999**, *30*, 155.
(7) Bordiga, S.; Palomino, G. T.; Zecchina, A.; Ranghino, G.; Giamello, E.; Lamberti, C. *J. Chem. Phys.* **2000**, *112*, 3859.
(8) Naderi, M.; Anderson, M. W. *Zeolites* **1996**, *17*, 437.
(9) Armaroli, T.; Busca. G.; Milella, F.; Bregani, F.; Toledo, G. P.; Nastro, A.; De Luca, P.; Bagnasco, G.; Turco, M. *J. Mater. Chem.* **2000**, *10*, 1699.
(10) Braunbarth, C. M.; Hillhouse, H. W.; Nair, S.; Tsapatsis, M.; Burton, A.; Lobo, R. F.; Jacubinas, R. M.; Kuznicki, S. M. *Chem. Mater.* **2000**, *12* (7), 1857.
(11) Cruciani, G.; De Luca, P.; Nastro, A.; Pattison, P. *Microporous Mesoporous Mater.* **1998**, *21*, 143.
(12) Nair, S.; Jeong, H.-K.; Chandrasekaran, A.; Braunbarth, C. M.; Tsapatsis, M.; Kuznicki, S. M. *Chem. Mater.* **2001**. In press.

10.1021/ja011703z CCC: $20.00
Published on Web 11/30/2001

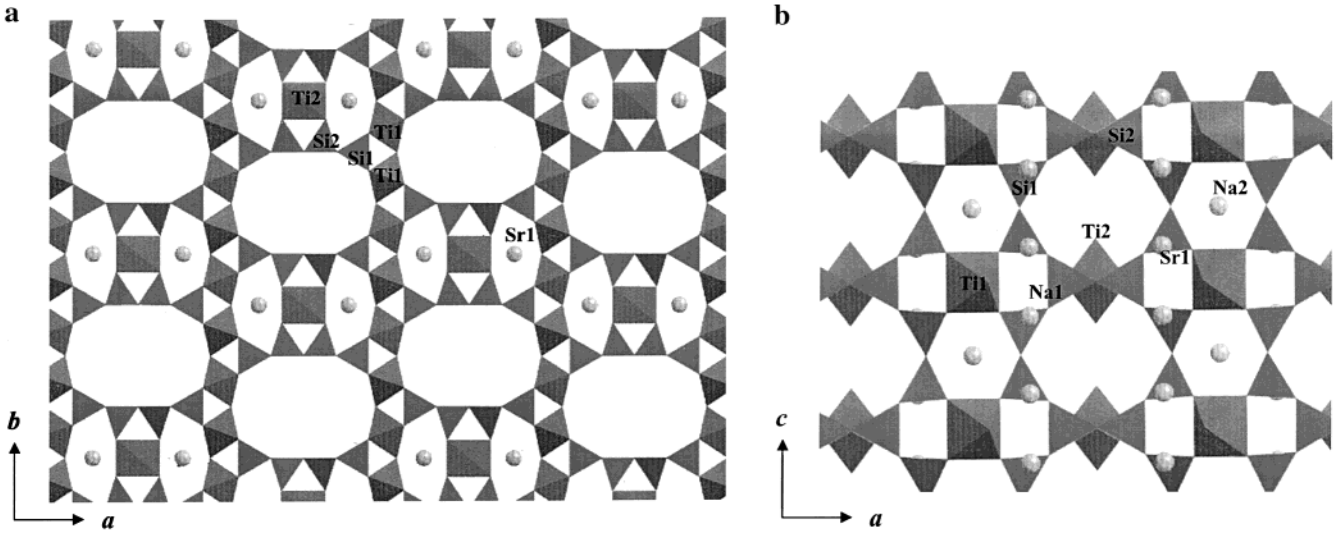

Figure 1. (a) View of the Na-ETS-4 framework down the [001] direction showing open 12-membered rings caused by AA-type stacking of bridging units along [001]. The ABAB-type stacking of the layers along [100] is also illustrated. Sodium cations are shown occupying the Na1 sites adjacent to the bridging units. The titania chains containing octahedrally coordinated titanium propagate along [010]. (b) View of the Na-ETS-4 framework down the [010] direction, showing the eight-membered silicate ring. Both sodium cation sites Na1 and Na2 (in the six-membered ring) are shown. Both the possible orientations of the five-coordinated Ti2 atom are shown in the figure.

chains by the same silicate tetrahedra that connect the chains in the [001] direction.

The above structural model implies that ETS-4 is the synthetic analogue of the titanosilicate mineral zorite.[14] Both ETS-4 and zorite are disordered crystalline materials, being faulted in the [100] and [001] directions. Crystallographically, their structure is described as an intergrowth of four polytypes[10] which differ in the stacking of the titanosilicate bridging units in the [100] and [001] directions. In the [100] direction, the bridging units can be stacked in either an ABAB or an ABCD-type sequence, whereas in the [001] direction they may be stacked in either an AA- or an AC-type arrangement, leading to a total of four possible polytypes. Figure 1a shows the view of the Na-ETS-4 framework down the [001] direction (sodium ions are shown, but not the occluded water molecules). In this view, the bridging units are stacked directly over each other in an AA sequence in the [001] direction, leading to open 12MR channels down [001]. However, if alternate framework layers in the [001] direction are shifted with respect to each other by 0.5*b*, we obtain an AC-type stacking down [001], causing a blockage of the 12MR channels. Figure 1a also shows one possible arrangement of the bridging units along [100], clearly an ABAB-type stacking. The as-synthesized ETS-4 framework can be modeled in the *Cmmm* space group as a superposition of the four polytypes, with a statistical distribution of the titanosilicate bridging units in the framework.[10]

Figure 1b shows a view down the [010] direction, which has 8MRs. While the 12MR channels in ETS-4 are blocked for reasons mentioned above, the faulting does not block the 8MR channel. Therefore, ETS-4 is expected to possess molecular sieving properties similar to those of small-pore zeolitic materials. Figure 2 shows three clusters belonging to the ETS-4 structure: (a) an eight-membered ring (8MR), (b) a bridging titanosilicate unit with a five-coordinated titanium atom, and (c) a titania chain with three-membered titanosilicate rings. Two of these rings share a common edge and are related by mirror symmetry, and we refer to them as double three-membered rings (D3MRs) to distinguish them from the titanosilicate 3MR in the bridging unit (Figure 2b). Most of the atoms are labeled for clarity, and the unlabeled atoms can be easily recognized as symmetry copies[12,13] of the labeled atoms.

As mentioned earlier, the as-synthesized Na-ETS-4 form is thermally unstable, and the structure collapses upon heating to temperatures in excess of 473 K. It can, however, be used in low-temperature applications such as in the form of a pervaporation membrane[15] for alcohol/water separations. A strontium ion-exchanged form of ETS-4 (Sr-ETS-4)[16] shows greater thermal stability. In this framework, the divalent strontium ions occupy only the Na1 sites[10] of Figure 1a. More than two-thirds of the Na2 site cations (Figure 1b) are also exchanged out of the structure to satisfy charge balance. Sr-ETS-4 has recently found application in the room-temperature separation of small molecules of nearly equal size (such as N_2/CH_4 and N_2/O_2), by a mechanism which is termed the "molecular gate" effect.[17] This term has been proposed to describe the continuously tunable effective dimension of the 8MR of Sr-ETS-4, leading to the possibility of separating different sets of molecules with the same material. This tunability is achieved by heat-treating the crystalline material at different temperatures.[17] Based on this effect, a new N_2/CH_4 separation process employing Sr-ETS-4 is under commercialization by Engelhard Corporation.

Thermogravimetric measurements[17] have shown that upon heat treatment of Sr-ETS-4, surface water and loosely bound structural water molecules leave the crystals at temperatures below 373 K. In this temperature range, powder X-ray diffraction patterns[17] show a small, continuous shrinkage of the unit cell with increasing heat-treatment temperature. Beyond 373 K, there is a second loss of water molecules strongly bound to the cations, leading to a larger shrinkage in the unit cell dimensions between 373 and 403 K. At still higher temperatures, there is again a continuous shrinkage in the unit cell dimensions, the

(13) Sandomirskii, P. A.; Belov, N. V. *Sov. Phys. Crystallogr.* **1979**, *24* (6), 686.

(14) *International Tables for Crystallography*; Hahn, T., Ed.; Space Group Symmetry, Vol. A; Kluwer: Dordrecht, 1995.

(15) Braunbarth, C. M.; Boudreau, L. C.; Tsapatsis, M. *J. Membr. Sci.* **2000**, *174* (1), 31.

(16) Kuznicki, S. M.; Bell, V. A.; Petrovic, I.; Desai, B. T. Small-Pored Crystalline Titanium Molecular Sieve Zeolites and Their Use in Gas Separation Processes. WO9932404A1, 1999.

(17) Kuznicki, S. M.; Bell, V. A.; Nair, S.; Hillhouse, H. W.; Braunbarth, C. M.; Jacubinas, R. M.; Toby, B. H.; Tsapatsis, M. *Nature* **2001**, *412*, 720.

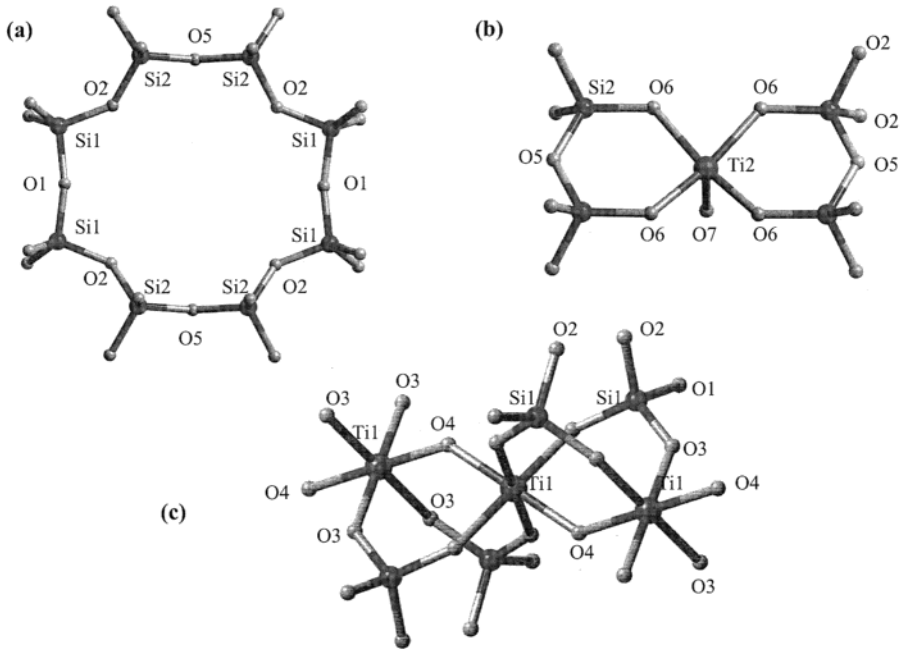

Figure 2. Representative clusters of the ETS-4 framework: the silicate 8MR (a), the titanosilicate bridging unit with a five-coordinated titanium (b), and a titania chain with the titanosilicate D3MRs also shown.

contraction finally becoming rapid near a heat-treatment temperature of about 573 K. At the same time, increasing levels of noncrystallinity are observed in the diffraction patterns as broad peaks. The framework contraction is reversible for samples treated at temperatures below approximately 523 K, and the crystals can re-adsorb atmospheric water to regain their original structure. Beyond this heat-treatment temperature, the framework contraction becomes irreversible (or very slowly reversible), the samples being stable in moist air for at least two weeks. In the heat-treatment temperature range of 550−600 K, Sr-ETS-4 becomes selective for N_2 (Pauling dimensions 4.1 Å in length and 3.0 Å in width) over CH_4 (4.2 Å in diameter), essentially excluding the latter from the framework while continuing to adsorb the former (about 15 cm^3 STP/gm at a pressure of 100 psi and a heat-treatment temperature of 550 K).[17] The O_2/Ar separation is also observed, although with a modest selectivity of about 5 at a heat-treatment temperature of 573 K. Heat treatment above 600 K leads to complete loss of crystallinity.

Although changes in the crystal structure play a role in initiating the size-selective behavior of Sr-ETS-4 samples heat-treated at higher temperatures, the mechanism by which this occurs is not well understood. Three major effects appear to be important in this situation: (1) distortive contraction of the framework upon dehydration, (2) disorder and loss of crystallinity in the framework due to the removal of the stabilizing water molecules, and (3) relocation of the Sr^{2+} cations in the framework. The first effect is manifest in the shrinkage of the unit cell dimensions. The second is consistent with the appearance of a broad amorphous peak and the broadening of crystalline peaks, in powder diffraction patterns (for example, Figure 2). The third effect is known in previously studied cases of framework deformation in dehydrated zeolitic frameworks.[18−21] We describe here an investigation of structural changes in dehydrated Sr-ETS-4. Powder neutron diffraction data from heat-treated Sr-ETS-4 samples have been analyzed by the Rietveld method to determine the structures of Sr-ETS-4 heat-treated at different temperatures. The crystallographic study is supported by the use of FT-Raman spectroscopy to probe the local structural deformations and disorder in the framework. Energy minimization simulations have also been used to investigate the relocation of the cations in the framework upon dehydration.

Experimental Section

Ion-exchanged Sr-ETS-4 was obtained from Engelhard Corporation. Samples (approximately 5 g) were heat-treated for 24 h at 423, 473, 523, and 573 K in Pyrex glass vials, through which a dry (<10 ppb water) helium stream was passed during the dehydration process. The vials were then sealed, and the samples were transferred to indium-sealed vanadium cans under a dry helium atmosphere before data collection. Room-temperature neutron diffraction patterns were collected between 6 and 130° 2θ on the high-resolution BT-1 powder diffractometer at NIST (Gaithersburg, MD), operating at a wavelength of 2.0783 Å with a Ge(311) monochromator and a 15′ Soller collimator for high neutron flux. The diffraction patterns were analyzed in the range 15−100° 2θ using the GSAS Rietveld refinement package.[22] Energy minimization simulations were performed with the *Cerius*^{2} package (Molecular Simulations, Inc.) employing the Universal Force Field.[23] The electrostatic charges on the framework atoms and cations were assigned by a charge equilibration calculation. FT-Raman spectra in the wavenumber range 75−1100 cm^{-1} were collected on heat-treated samples under a dry nitrogen atmosphere, using a Bruker FT-Raman spectrometer equipped with a Nd:YAG laser, at a resolution of 1 cm^{-1}. The heat-treated samples were packed into the cavity of an aluminum sample holder for data collection. A total of 256 scans were collected for each sample.

Results and Discussion

A. Rietveld Refinement. The neutron diffraction patterns of the dehydrated samples retain the orthorhombic *Cmmm* space

(18) Nenoff, T. M.; Parise, J. B.; Jones, G. A.; Galya, L. G.; Corbin, D. A.; Stucky, G. D. *J. Phys. Chem.* **1996**, *102*, 14256.
(19) Johnson, G. M.; Reisner, B. A.; Tripathi, A,; Corbin, D. R.; Toby, B. H.; Parise, J. B. *Chem. Mater.* **1999**, *11*, 2780.
(20) McCusker, L. B. *Zeolites* **1984**, *4*, 51.
(21) Baur, W. H.; Bieniok, A.; Shannon, R. D.; Prince, E. *Z. Kristallogr.* **1989**, *187*, 253.
(22) Larson, A. C.; von Dreele, R. B. Report LAUR 86-784, Los Alamos National Laboratory: Los Alamos, NM, 1986.
(23) Rappe, A. K.; Casewit, C. J.; Colwell, K. S.; Goddard, W. A., III; Skiff, W. M. *J. Am. Chem. Soc.* **1992**, *114*, 10024.

Table 1. Contraction of the Unit-Cell Parameters of Sr-ETS-4 with Increasing Heat-Treatment Temperature

heat-treatment temperature (K)	*a* (Å)	*b* (Å)	*c* (Å)
rt (ref 10)	23.1962(12)	7.2381(3)	6.9652(3)
423	23.0271(32)	7.0473(7)	6.6670(7)
473	23.0030(28)	6.9670(9)	6.6471(9)
523	22.9683(31)	6.8231(12)	6.6377(15)
573	22.9250(26)	6.6121(15)	6.5975(24)

group symmetry of the room-temperature structure. The patterns were first analyzed with the Le Bail structureless profile fitting algorithm,[24] to determine the unit cell and profile parameters. The broad amorphous peak (due to incoherent scattering) occurring in the diffraction patterns of the heat-treated samples is fitted as background[25] so that only the crystalline component of the sample is analyzed by Rietveld refinement. Shifted Chebyshev polynomials[22,32] with 24−30 coefficients were used to represent the background in the refinements reported here. The peak shape was modeled by a pseudo-Voigt function. Table 1 shows the final refined unit cell parameters of Sr-ETS-4 dehydrated at various temperatures. It is apparent that the framework at 423 K has undergone a large contraction with respect to the hydrated framework, with significant decreases (>0.15 Å) in the dimensions of all three crystal axes. This is followed by a gradual contraction up to 523 K, during which the *b*-axis shows the largest decrease in dimension while the *a*- and *c*-axes contract slowly. At 573 K there is a second large contraction, in which the *b*- and *c*-axes both decrease appreciably in dimension. To ascertain the location of the Sr^{2+} ions and residual water molecules, Fourier difference maps were constructed from the diffraction pattern of the sample heat-treated at 423 K, using a completely empty ETS-4 framework model with no cations or water molecules. Four difference peaks were observed in the void space of ETS-4. On the basis of the coordination environment and peak shape, three of these peaks are identified as Sr^{2+} positions. One position (Sr1, see Supporting Information, Table 1) is the same as that in the hydrous structure but has a low occupancy. The second site (Sr2) has a high occupancy and represents the movement of the ions in the *c*- and *a*-directions to enter the space between the titanosilicate D6MRs seen in Figure 1b. The third position (Sr3) represents the movement of the Sr^{2+} ions into the eight-membered ring of ETS-4. The fourth peak is interpreted as a residual water molecule, due to its coordination environment (a distance of about 2.1 Å from the heavily occupied Sr2 site, and a distance of about 3 Å from the apical oxygen of the titanosilicate bridge) and owing to the observation that this peak decreases regularly in intensity for samples heat-treated at higher temperatures. In the hydrated structure, water molecules occupied the Sr2 and Sr3 positions. Fourier difference maps of the diffraction patterns from samples heat-treated at higher temperatures do not show further relocation sites of the cations.

Energy-minimization simulations were carried out with all the four pure polytypes of ETS-4, using a $2 \times 2 \times 2$ supercell. The four polytypes were created by specifying the arrangement of the titanosilicate bridging units. The water molecules were completely removed from the frameworks, and the Sr^{2+} cations were distributed in the Sr1 site, obeying overall charge balance considerations. To allow movement of the cations out of their *Cmmm* special positions, the symmetry operations of the space group were not imposed in the simulations. However, the unit cell was constrained to the orthorhombic cell obtained from the Le Bail fit[24] for the sample heat-treated at 423 K. Upon relaxation of the lattice, the cations converge to essentially the same positions (Sr1, Sr2, and Sr3) as described above, supporting the existence of these coordination sites in the dehydrated frameworks. Since the relaxed lattices become rather disordered due to the removal of crystal symmetry, the Sr···O coordination distances in these relaxed structures show a wider distribution than would be obtained from a symmetry-constrained structure. Qualitatively, the Sr···O contacts in the relaxed structures were found to vary between 2.4 and 2.8 Å for Sr1, and between 2.7 and 3.2 Å for Sr2 and Sr3. These distances are in approximate agreement with those obtained after the Rietveld fitting was completed (Figure 5f).

After locating the cation and residual water binding sites, Rietveld refinement of the heat-treated framework structures was carried out in the *Cmmm* space group, using the refined background and profile parameters from the structureless fit. The residual sodium ions remaining from the ion exchange (and which cannot be exchanged due to charge balance constraints) are also included in the refinement. The validity of performing Rietveld analysis using the superposition *Cmmm* structure has been established earlier.[10] In that study, a 2-D "faulting map" was prepared with the four pure polytypes at the corners. The edges and interior of the map are occupied by structures with various degrees of faulting in the *a*- and *c*-directions. Systematic simulations of the X-ray patterns of ETS-4 structures located at various points on the faulting map revealed that the experimental powder diffraction patterns were consistent with a structure at the center of the faulting map, which can therefore be represented as a random intergrowth of the four pure polytypes with *Cmmm* symmetry.

The atomic coordinates, occupancies, and isotropic atomic displacement parameters (ADPs) were refined. The heavy atoms (Sr, Ti, and Si) were refined with a single ADP for all atoms of the same element. This allows a reduction in the number of refined parameters and is justified by the absence of significant residual nuclear density around the heavy atoms in the difference Fourier maps. The oxygen atoms are refined with individual isotropic ADPs. The background, profile, and lattice parameters are also refined further and show minor improvements from the Le Bail fitted[24] values (Table 1 shows the final values after Rietveld refinement). A three-site occupancy constraint[26] was introduced for the Sr^{2+} cations, to satisfy both the overall charge balance as well as the total number of Sr^{2+} cations as known from chemical analysis of the room-temperature structure.[10] The so-called "channel coalescence" defect (characterized by missing titanosilicate bridging units) was also modeled by considering the bridge as a single unit for purposes of occupancy refinement. Hence, the occupancy parameters of the atoms comprising the bridging unit are constrained to the ratio 1 Ti2:2 Si2:4 O5:2 O6:1 O7. This occupancy parameter and the cation occupancies

(24) Le Bail, A.; Duroy, H.; Fourquet, J. L. *Mater. Res. Bull.* **1988**, *23*, 447.
(25) Young, R. A., Ed. *The Rietveld Method*; Oxford University Press: New York, 1993; pp 102−110.
(26) Joubert, J.-M.; Cerný, M.; Latroche, A.; Percheron-Guégan, A.; Yvon, K. *J. Appl. Crystallogr.* **1998**, *31*, 327.
(27) Nenoff, T. M.; Parise, J. B.; Jones, G. A.; Galya, L. G.; Corbin, D. R.; Stucky, G. D. *J. Phys. Chem.* **1996**, *100*, 14256.
(28) Mihailova, B.; Valtchev, V.; Mintova, S.; Konstantinov, L. *Zeolites* **1996**, *16*, 22.
(29) Astorino, E.; Peri, J. B.; Willey, R. J.; Busca, G. *J. Catal.* **1995**, *157*, 482.
(30) Dutta, P. K.; Rao, K. M.; Park, J. Y. *J. Phys. Chem.* **1991**, *95*, 6654.
(31) Ashtekar, S.; Prakash, A. M.; Kevan, L.; Gladden, L. F. *Chem. Commun.* **1998**, 91.
(32) Abramowitz, M., Stegun, I. A., Eds. *Handbook of Mathematical Functions*; U.S. Government Printing Office: Washington, DC, 1972; pp 771−795.

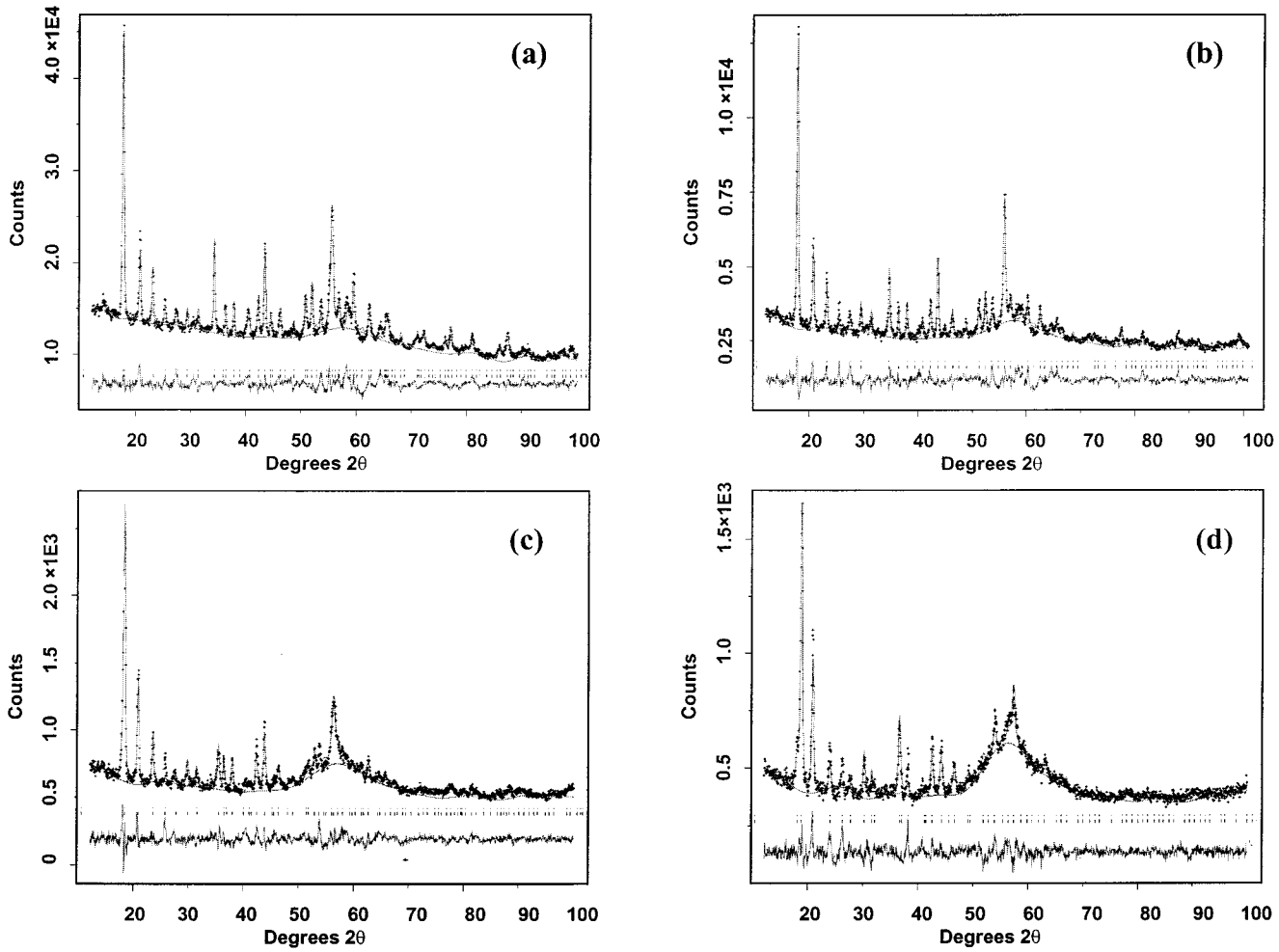

Figure 3. Best fits obtained from the neutron diffraction patterns from Sr-ETS-4 heat-treated in dry helium for 24 h at 423 K (a), 473 K (b), 523 K (c), 573 K (d). The fitted total intensity and the background curve (continuous lines) are superimposed on the observed pattern (+). The tick marks are possible *Cmmm* reflection positions. The difference profile is shown at the bottom.

were initially refined in alternate cycles, and then together in the final cycles to ensure charge neutrality. Soft constraints on the bond lengths (Si−O: 1.60 ± 0.05 Å and Ti−O: 2.0 ± 0.07 Å for the framework oxygens O1−O6 and 1.7 ± 0.05 Å for the apical oxygen O7) and bond angles (O−Si−O: 109.5 ± 7° and O−Ti−O: 90 ± 5°) were necessary throughout the refinement. These soft constraints allow deviations of the bond lengths and angles about physically reasonable values; the deviations are usually specified to be less than 5%. In the present case, removal of the soft constraints resulted in nonphysical bond lengths and angles. However, the soft constraint weight factor could be reduced to the point that the soft restraints contribute only 6% of the residual χ^2 at 423 K, increasing to 10% at 573 K. Lowering the soft constraint weight factors further led to nonphysical bond distances and angles, whereas higher weights increased the residuals, with a poor fit of the data. Also, the complete removal of the soft constraints from the fit gave only small improvements (<0.1%) in the residuals when compared to the results reported here. In view of this difficulty, it was decided to proceed with constrained refinements and interpret their results in a consistent and physically reasonable manner. Restrained refinements have previously been used to obtain information on the structural changes in dehydrated zeolitic frameworks.[27] The refined structural parameters for all of the heat-treated structures are available in Supporting Information, Table 1, whereas Figure 3,a−d, shows the corresponding fitted profiles. Figure 4, a,b, shows the structure of Sr-ETS-4 dehydrated at 573 K, with the relocated cations (large spheres) and water molecules (small spheres) also shown.

B. Structure of Dehydrated Sr-ETS-4. Several features of the framework contraction are deduced from Figure 5, a−f, which represent the bond geometry of the heat-treated frameworks. The Si−O bond distances shown in Figure 5a have physically reasonable values around 1.6 Å, which do not show large systematic variations as a function of heat-treatment temperature. However, the Ti−O bond distances in Figure 5a show more interesting behavior. In particular, the Ti1−O3 and Ti1−O4 bond lengths in the D3MR structures of Sr-ETS-4 show large changes in their values, whereas the Ti2−O6 bond associated with the 3MR structures in the bridging unit shows very little change as a function of heat-treatment temperature. Changes in the bond lengths consistent with Figure 5a are also suggested by the Raman spectroscopy results discussed in a following section. We also note (see Supporting Information, Table 1) that the five-coordinated Ti2 atom in the bridging unit approaches the special position ($z = 0$) with increasing heat-treatment temperature, that is, the Ti2 of the bridging unit and four O6 atoms bonded to it approach a square-planar geometry. The apical Ti2−O7 bond length remains essentially constant at about 1.7 Å. A six-coordinated bridging titanium in hydrous Na-ETS-4 has also been proposed from a powder X-ray structure refinement,[11] with the Ti2 atom located in the mirror plane of *Cmmm* perpendicular to the *c*-axis. However, the reliability of that result is uncertain since the Ti2:O7 ratio in that refined

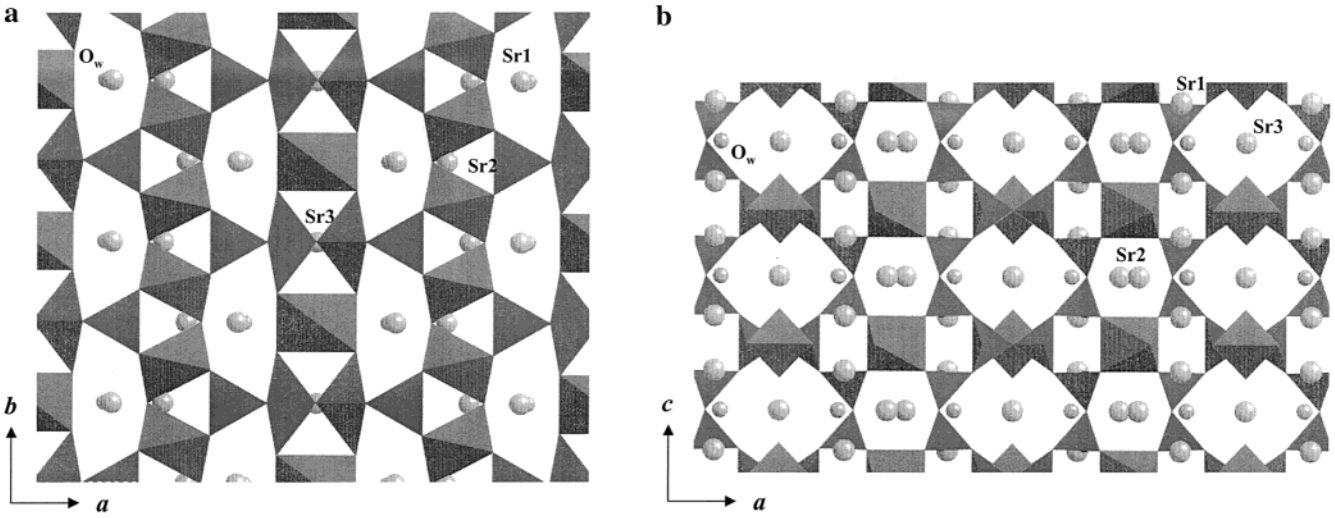

Figure 4. Structure of Sr-ETS-4 heat-treated at 573 K, (a) viewed down [001], and (b) down [010]. The strontium ions and residual water position are also labeled.

structure is 1:4.8, a physically unreasonable value. As mentioned earlier, the Ti2:O7 ratio is constrained to 1:1 (i.e., a five-coordinated titanium) in the present refinements based on the previous data, and is supported by the fact that the difference Fourier synthesis is featureless to 0.01 $Å^{-3}$ within a radius of 1 Å around the O7 position. The isotropic ADP for O7 also has a quite reasonable value (Supporting Information, Table 1, also see Figure 5e). If the Ti2:O7 ratio were 1:2, the ADP (which has a strong positive correlation with the occupancy) would have to be refined to an unreasonably large value to support the doubling in occupancy of O7.

The O−Si−O and O−Ti−O bond angles are shown in Figure 5b, where it is noted that the average O3−Ti1−O4 angle shows a steady increase with increasing heat-treatment temperature. This bond angle is within the D3MR titanosilicate ring, which is formed by coordinating two silicate tetrahedra to the O−Ti−O chains. A 3MR (with two silicon atoms and one titanium atom at the corners) is also found in the bridging unit, and the O6−Ti2−O6 angle in this 3MR also increases with increasing heat-treatment temperature. Both the D3MR and the 3MR are expected to be strained in the room-temperature structure, and the loss of crystallinity in the material at higher temperatures is likely to originate from the breakage of T−O bonds in these rings. The Si−O−Si and Ti−O−Ti angles (Figure 5c) show a greater spread when the heat-treatment temperature is increased. The average Ti1−O4−Ti1 angle shows a steady decrease with increasing heat-treatment temperature. This corresponds to the crumpling of the O−Ti−O chains and the shrinkage of the crystallographic *b*-dimension. The average Si1−O1−Si1 angle passes through 180°, which is significant for understanding the distortion of the 8MR as explained in a following section. Figure 5d shows the O−O distances in the framework. The O−O distances in the D3MR (shown as O3−O4(1)) and in the 3MR (shown as O6−O6(1)) increase considerably with increasing heat-treatment temperature. As a result, the O3−O4 and O6−O6 distances between neighboring D3MRs (shown as O3−O4(2)) and between neighboring 3MRs (shown as O6−O6(2)) fall to low values at high heat-treatment temperatures (bottom right corner of the Figure).

Hence, the D3MR (Ti1−O4−Ti1−O3−Si1−O3−Ti1) shows an increasing O3−Ti1−O4 angle, a decreasing Ti1−O4−Ti1 angle, and an decreasing inter-ring O3−O4 distance, as mentioned previously. Similarly, the 3MR (Ti2−O6−Si2−O5−Si2−O6−Ti2) has an increasing O6−Ti2−O6 angle and a decreasing inter-ring O6−O6 distance. Figure 5e shows the isotropic ADPs (U_{iso}) for the framework oxygen atoms O1 to O6, as a function of the heat-treatment temperature. The two highest ADPs for a heat-treatment temperature of 573 K are those for O4 and O1. The large and rapidly increasing ADP for O4 suggests that it is highly disordered about its average crystallographic position in *Cmmm*. This disorder exists because the −O4−Ti1−O4- chains do not crumple uniformly along the *b*-axis upon heat-treatment. Rather, there is a broad distribution of O4 positions in the heat-treated samples. The large ADP for O4 is also related to the irreversibility of the framework contraction at higher heat-treatment temperatures. When the O4 atom displays a large degree of disorder about its average position, it is likely that a significant number of Ti1−O4 bonds can be considered as being no longer of a strong covalent nature, leading to an irreversible framework contraction. On the other hand, O6 has a slowly increasing ADP, suggesting that the 3MR of the bridging unit remains relatively stable upon heat treatment. The occupancy of the bridging unit also remains essentially constant with heat-treatment temperature. The disorder of O1 is related to the contraction of the effective dimensions of the 8MR, as will be discussed below.

The coordination environments of the three Sr^{2+} ions and the water molecules have also been examined (Figure 5f). The ionic radii of oxygen (1.26 Å) and strontium (1.32 Å) add up to 2.58 Å, giving an approximate lower bound on chemically reasonable Sr···O distances. On the basis of this consideration, the distances reported in Figure 5f involving the Sr2 and Sr3 cations seem to be valid. However, the distances involving the Sr1 cation appear to be rather low, especially the (crystallographic average) Sr1···O4 distance which decreases steadily with increasing heat-treatment temperature and is about 2 Å for a heat-treatment temperature of 573 K. This rather low average Sr1···O4 distance is not an indication of unreliability of the refined structure but is a result of the fractional occupancy of the Sr1 cation site and the disorder in the position of the O4 atom. The O4 atom in this case has large static disorder, with an RMS displacement of about 0.9 Å from its average *Cmmm* position (as indicated by its isotropic ADP of 0.8 $Å^2$). Moreover, the cation site Sr1 is itself fractionally occupied in the heat-treated frameworks (Supporting Information, Table 1), with an occupancy of only about 0.2 ("40%"), as opposed to a maximum crystal-chemically reasonable occupancy of 0.5 ("100%") or the actual occupancy[10] of 0.483 ("96.6%") in the hydrous structure.

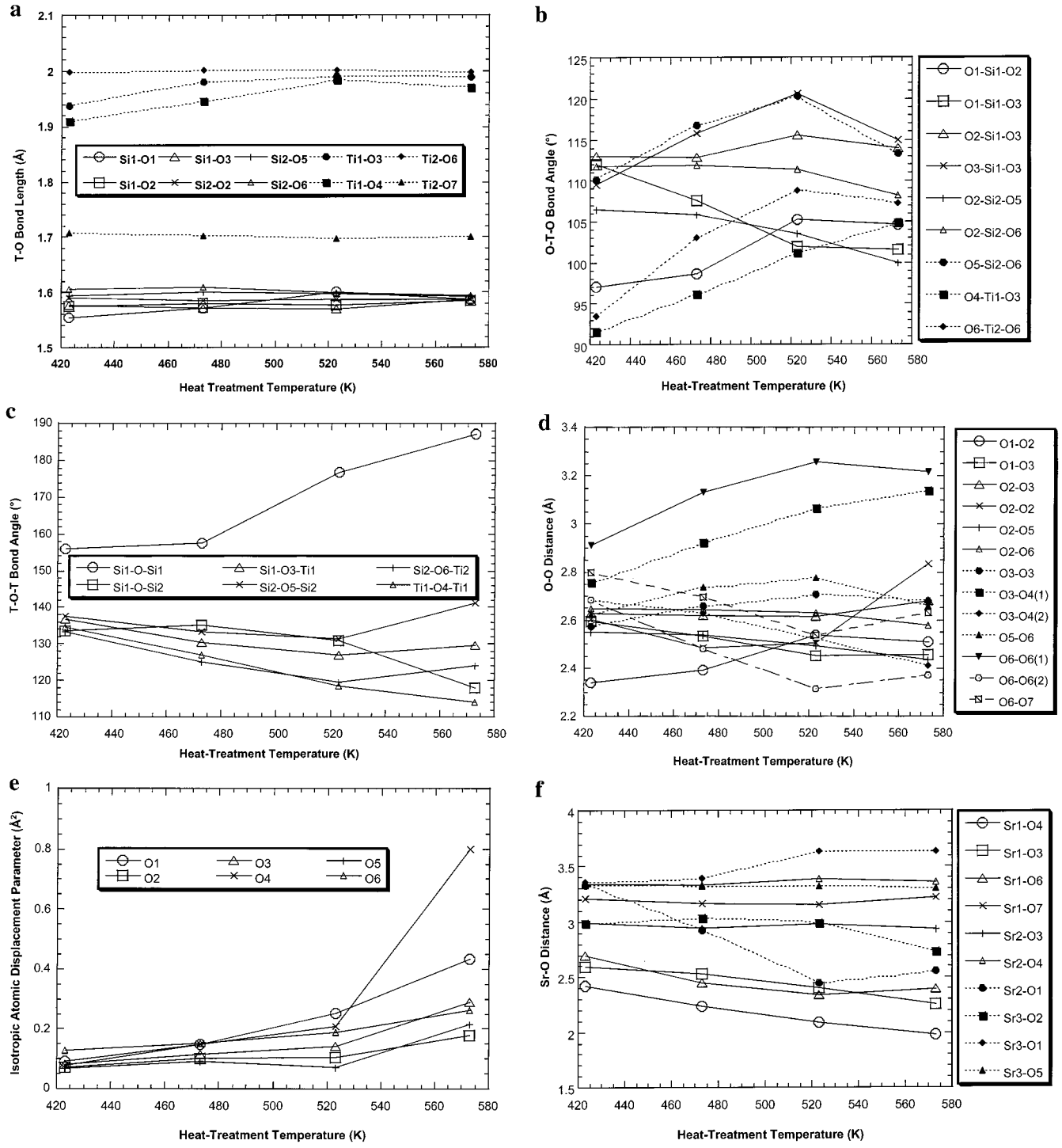

Figure 5. Geometrical details of heat-treated Sr-ETS-4 structures, showing T−O (T = Si, Ti) bond distances (a), O−T-O bond angles (b), T−O-T bond angles (c), O−O distances (d), Isotropic thermal parameters for oxygen atoms (e), and Sr−O coordination distances (f). The Rietveld estimated standard deviations (esd) on the bond length are less than 0.01 Å in all cases, and less than 0.1° on the bond angle in all cases.

Hence, the actual Sr1···O4 distance at an occupied Sr1 site can be quite different from the crystallographic average distance. However, this low-average Sr1···O4 distance does reflect the fact that a large occupancy of the Sr1 site is not favorable in the heat-treated structures, leading to relocation of the Sr1 cations to Sr2 and Sr3 sites. We suggest that presence of the Sr^{2+} cations at the Sr1 and Sr2 sites promotes the stability of the framework by restricting the bending of the Ti1−O4−Ti1 angle and stabilizing the D3MRs. In the case of Na-ETS-4, it may be hypothesized that the smaller Na^{+} cations exercise less influence on the framework distortion and are unable to prevent its collapse at relatively low heat-treatment temperatures. In view of this hypothesis, a comparative study of framework stability and cation relocations in various ion-exchanged ETS-4 materials is of interest and is presently underway. The locations of the Sr^{2+} cations show no significant changes after the initial relocation at 423 K, but the occupancy of the Sr3 site increases to about 0.37, so that slightly more than a third of the 8MRs are blocked by Sr^{2+} cations. Turning to the occupancy of the residual water molecule (O_w), we note (Supporting Information, Table 1) that its refined occupancy decreases significantly with increasing heat-treatment temperature, which is the expected

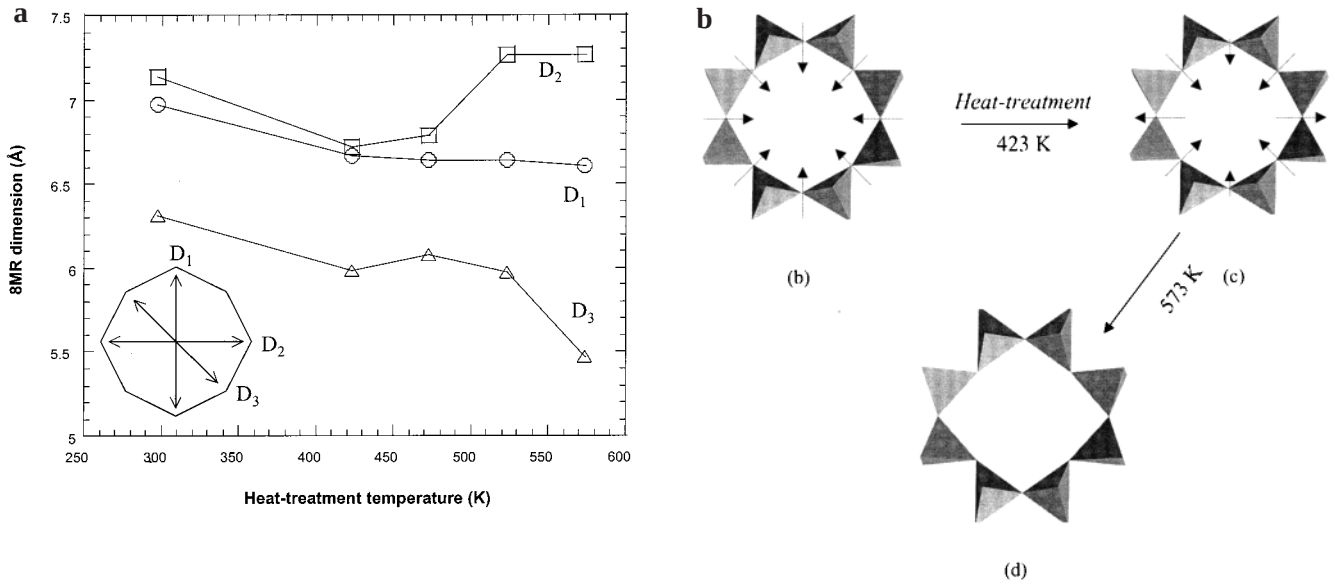

Figure 6. Evolution of the dimensions D_1, D_2, and D_3 (see schematic, inset) of the 8MR of Sr-ETS-4 upon heat-treatment (a). D_1 is along the crystallographic *c*-axis and D_2 is along the *a*-axis. The 8MR of hydrous Sr-ETS-4 (b), Sr-ETS-4 after heat-treatment at 423 K (c), and after heat-treatment at 573 K (d). The movements of the oxygen atoms upon increasing the heat-treatment temperature are indicated in (b−c).

behavior. The water molecule tends to show a drift in the *a*-direction with increasing heat-treatment temperature, and appears to be following the Sr2 cation as it moves nearer the D6MR.

C. The 8MR in Sr-ETS-4. The behavior of the 8MR has an important role in determining the separation properties of Sr-ETS-4. The dimensions of the 8MR are described by the three distances D_1 (O5−O5), D_2 (O1−O1), and D_3 (O2−O2), which are plotted in Figure 6a as a function of heat-treatment temperature. Figure 6 also shows the 8MR (as viewed down [010]) in hydrous Sr-ETS-4[10] (b), Sr-ETS-4 heat-treated at 423 K (c), and at 573 K (d). Figure 6, b and c, also shows the movements (dotted lines) of the oxygen atoms in the 8MR as the heat-treatment temperature is further increased. D_1 is identical to the lattice parameter *c*, which strictly decreases upon increasing the heat-treatment temperature. Upon heat treatment at 423 K, all three distances shrink considerably from their room-temperature values. The slopes of all three lines in Figure 6d are almost identical in this temperature range, so that the 8MR only decreases in size but does not change in shape, as indicated also by the direction and relative magnitudes of the movement of the oxygen atoms (Figure 6b,c). The dimension D_3 is the smallest dimension of the 8MR and hence is expected to control the transport characteristics. Between 423 and 473 K, D_2 and D_3 increase slightly, whereas D_1 continues to contract slowly. Beyond 473 K, D_3 contracts rapidly, whereas the horizontal dimension D_2 expands relatively, so that the 8MR distorts from an "octagonal" toward a "quadrilateral" cross section. During this process, the average Si1−O1−Si1 angle passes through 180° (Figure 5c), and this process seems to be accompanied by disorder in the position of O1 as seen from the increase in its ADP (Figure 5e). The molecular sieving properties of the material are expected to be largely dependent on the limiting dimension D_3, which exhibits a rather nonmonotonic behavior with increasing heat-treatment temperature (Figure 6a). This should be reflected in the heat-treatment temperature dependence of the size- and shape-selectivity behavior in various types of small-molecule separations.

D. Vibrational Spectra of Heat-Treated Sr-ETS-4. In this section we consider some features of Raman spectra obtained from Sr-ETS-4 dehydrated at various heat-treatment temperatures. Vibrational mode assignments for Raman and infrared absorption spectra of Na-ETS-4 have been attempted previously in two publications, based on group-frequency comparisons[9] with other titanosilicate materials,[29] and on force-field calculations of model clusters[28] taken from the ETS-4 structure. Figure 7 shows FT-Raman spectra of hydrous Na-ETS-4 (a), hydrous Sr-ETS-4 (b), and Sr-ETS-4 after heat treatment at the same temperatures as examined by neutron diffraction analysis (c−f). The Raman spectra of hydrous Na-ETS-4 and Sr-ETS-4 (a−b) have a broad, weak band around 1050 cm^{-1}, which is due to the asymmetric stretching of the Si−O−Si bridges. This vibrational mode is weak in the Raman spectrum due to its small polarizability variation. There is a split peak between 900 and 930 cm^{-1}, which is due to the stretching vibrations of the Si−O−Ti bridges[29] found in the D3MR and the 3MR of ETS-4. The lower-frequency component can be ascribed to the symmetric stretching mode (which is accompanied by an in-plane deformation), whereas the higher-frequency component is assigned to the asymmetric Si−O−Ti stretching vibration. This peak broadens somewhat upon increasing the heat-treatment temperature, probably due to disorder in the O3 atoms, as indicated by its increasing isotropic ADP (Figure 5e). The intense peak at 740−760 cm^{-1} is attributed to the Ti−O−Ti symmetric stretch, involving the oxygen atom O4 in the titania chains. This peak is shifted downward in frequency by about 15 cm^{-1} in hydrous Sr-ETS-4 (b), when compared to hydrous Na-ETS-4 (a). The shift is due to the increased interaction of the O4 atom with the larger Sr^{2+} cation in the heavily occupied Sr1 site (Sr1···O4 distance[10] = 2.517(7) Å). This peak also broadens and decreases in frequency with increasing heat-treatment temperature, the largest change taking place between 423 and 473 K. The broadening of this vibrational band upon heat-treatment is explained by the disorder of the O4 atom in the Ti1−O4−Ti1 chains, consistent with the rapidly increasing isotropic ADP of the O4 atom (Figure 5e). The decrease in the peak frequency with increasing heat-treatment temperature is consistent with the considerable increase in the Ti1−O4 bond length (Figure 5a) induced by heat-treatment.

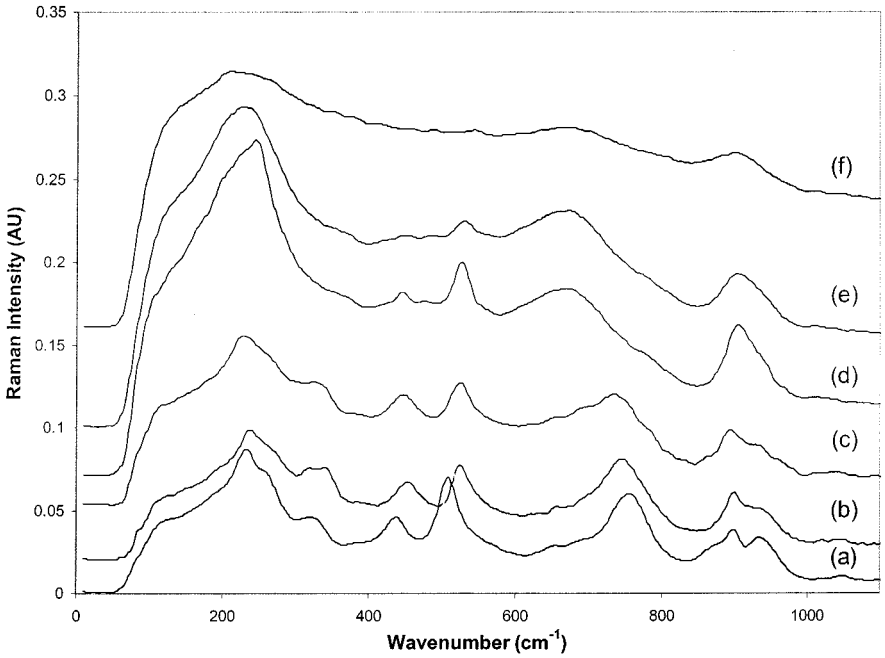

Figure 7. Room-temperature FT-Raman spectra of hydrous Na-ETS-4 (a), hydrous Sr-ETS-4 (b), and Sr-ETS-4 after heat-treatment for 24 h in dry helium to 423 K (c), 473 K (d), 523 K (e), and 573 K (f).

The assignment of the two peaks between 400 and 550 cm^{-1} is unclear from previous investigations, which are summarized as follows. Vibrational calculations (using an ETS-4 cluster similar to that shown in Figure 2c) indicate that the peaks at approximately 515 and 445 cm^{-1} can be interpreted as Ti1−O4−Ti1 and O4−Ti1−O4 bending modes in the titania chains,[28] which form one edge of the D3MRs of ETS-4 (Figure 2c). On the other hand, these peaks have also been tentatively assigned[9] to the symmetric stretching vibrations of the Ti1−O3−Si1−O3−Ti1 species of the D3MRs. Additionally, there exists an empirical correlation,[30,31] between the size of the ring units (i.e., 3MR, 4MR, etc.) of zeolitic frameworks and their characteristic ring deformation frequencies, involving primarily the in-plane motion of the oxygen atoms. According to this correlation, the frequency of the ν_s (T−O−T) ring deformation mode (T = Si, Al) has an inverse dependence on the magnitude of the average T−O−T angle in the ring. The T−O−T angle, in turn, usually increases with increasing ring size. Hence, the characteristic frequency of a ring unit in a zeolitic framework is expected to be inversely proportional to the number of atoms in the ring. 4MR ring structures in zeolites have this characteristic band between 470 and 510 cm^{-1}. In the titanosilicate material ETS-10, the Raman peak at 539 cm^{-1} was identified with the 3MR.[31] On the basis of the correlation, it was shown that this vibrational frequency (which is higher than the characteristic 4MR frequency in zeolites) would be consistent with an Si−O−Ti angle of magnitude similar to that in the 3MR of ETS-10 (about 130°), thus supporting the identification of this band with the 3MR unit. The 3MRs in ETS-10 are identical to those found in the ETS-4 bridging unit (Figure 2b). However, ETS-10 has no three-membered units of the type found in the D3MRs of ETS-4. While the 3MRs in ETS-10 and the bridging unit of ETS-4 contain only one Ti atom, the D3MR of ETS-4 contains two Ti atoms.

On the basis of the present data and the above discussion, we suggest that the Raman peak at 515 cm^{-1} can be associated with the D3MR in ETS-4, since the average Ti1−O4−Ti1 and Si1−O3−Ti1 angles in hydrous Sr-ETS-4[10] are both 135° and hence are close to the 3MR angles in ETS-10. In the present case, we also observe that this peak is shifted upward by about 15 cm^{-1} in hydrous Sr-ETS-4 when compared to hydrous Na-ETS-4. This is again attributed to the interaction of the Sr^{2+} cations with the D3MRs. In hydrous Sr-ETS-4, the heavily occupied Sr1 site is in the close vicinity of the D3MR and interacts strongly with the O4 atom (as also shown from the shift in the Ti1−O4 stretching band mentioned earlier), as well as with the O3 atom. These are the oxygen atoms found in the D3MRs of ETS-4 (Figure 2c). The Sr1 site cations would tend to decrease both the Si1−O3−Ti1 and Ti1−O4−Ti1 angles in the D3MR by attracting the O3 and O4 atoms, thus shifting the characteristic D3MR band upward in frequency, in comparison to hydrous Na-ETS-4. However, this also means that the Raman frequency shift due to cation substitution does not allow us to distinguish whether this vibrational mode involves the motion of the O4 atom or the O3 atom.

If the characteristic D3MR peak at 515 cm^{-1} is indeed due to the bending mode of the Ti1−O4−Ti1 species of the D3MR as previously suggested,[28] it is surprising that this peak shows very little change in frequency upon heat-treatment (a slight increase of about 7 cm^{-1} between heat-treatment temperatures of 423 and 573 K). This is inconsistent with the fact that the average Ti1−O4−Ti1 angle decreases by as much as 20° between these two heat-treatment temperatures (Figure 5c). Second, we must consider the fact that the Sr1 site is no longer heavily occupied in the heat-treated structures. However, the O3 atom continues to interact with the heavily occupied Sr2 site in the heat-treated structures. This is clear from Figure 5f, which shows that the Sr2···O3 distance is about 3.0 Å in the heat-treated structures. The O4 atom interacts only weakly with Sr2, since the average Sr2···O4 distance is about 3.3 Å in the heat-treated structures. Hence, the present data indicate that the characteristic deformation mode of the D3MR at 515 cm^{-1} probably involves in-plane motion of the O3 atom connecting the Si1 and Ti1 atoms in the D3MR, rather than the O4 atom. Since the motion of the O3 atom is coupled to the motion of the Ti1 and Si1 atoms, the in-plane deformation mode would be split into two components[29]—a symmetric stretching component (observed at 515 cm^{-1}) and a Si1−O3−Ti1 bending

component (observed at 445 cm^{-1}). As expected, these modes broaden out upon increasing the heat-treatment temperature due to the disorder in the atoms constituting the D3MRs.

The peak visible around 330 cm^{-1} may be interpreted as a Ti−O−Ti bending vibration.[9,28] Due to the broadness and low intensity of this peak, its frequency shift due to cation substitution and heat-treatment could not be reliably determined. However, it appears to lose intensity with increasing heat-treatment temperature, suggesting that it is a bending mode involving the titania chains as indicated by vibrational mode calculations. The intense peak around 230 cm^{-1} has been assigned[9] to the out-of-plane rocking vibration of the Ti1−O4−Ti1 chains. However, it was also reported[28] that this mode could not be modeled as a vibration involving only one type of heavy atom (i.e., Si or Ti alone), but was found to be due to a Si−O−Ti bending vibration. Furthermore, a Ti−O−Ti rocking mode is expected to have low intensity in the Raman spectrum and high intensity in the infrared absorption spectrum,[29] whereas the opposite behavior was found for this band in ETS-4.[9,28] Hence, this peak is more likely to represent the Si1−O3−Ti1 bending mode.

In conclusion, the interpretation of the Raman spectra of heat-treated samples confirms that the D3MRs in ETS-4 are unstable upon heat-treatment, leading to the crumpling of the titania chains and accompanying disorder in the O4 atom. This is reflected in the behavior of the Ti−O−Ti stretching mode. Furthermore, the effect of cation substitution in ETS-4 enables the identification of the peak at 515 and 445 cm^{-1} with a characteristic deformation mode of the D3MR, which appears to involve mainly the motion of the O3 atom. Disorder in the ETS-4 framework, induced by heat-treatment, also leads to broadening of the vibrational bands.

Conclusions

Knowledge of the framework contraction and cation relocation in heat-treated Sr-ETS-4 molecular sieves is of interest in understanding and controlling its separation properties. Toward this end, the present neutron diffraction results describe the structural changes in the framework, showing clearly the contraction in the effective dimensions of the 8MR, as well as the disordered contraction of the titania chains and the instability of the D3MRs. The relocation of the Sr^{2+} cations into three sites is also elucidated. Raman spectroscopy has been used to follow the framework structural changes, the results being in agreement with the refined crystallographic structures and reflecting the disordered nature of the heat-treated frameworks. Frequency shifts and intensity changes caused by cation-framework interactions and heat-treatment are also found to be useful in assigning vibrational modes in ETS-4.

Acknowledgment. We acknowledge funding from Engelhard Corporation and ATP/NIST (Cooperative Agreement 70NANB9H3036). We also thank the Materials Research Science and Engineering Center (MRSEC), University of Massachusetts Amherst, for use of their Raman spectroscopy facility.

Supporting Information Available: Atomic parameters for Sr-ETS-4 in space group *Cmmm* (PDF). This material is available free of charge via the Internet at http://pubs.acs.org.

JA011703Z